

## Particle collection by permeable drops

Robert H. Davis\* and Alexander Z. Zinchenko

*Department of Chemical and Biological Engineering University of Colorado Boulder Boulder,  
Colorado 80309-0596 USA*



(Received 18 July 2018; published 1 November 2018)

The interaction of a small, solid particle with a nearby fluid droplet covered with a thin, permeable membrane is considered for linear ambient flows under conditions where viscous forces dominate. A bispherical-coordinate solution was developed to describe the relative motion along and normal to the line-of-centers between the particle and drop. The effect of the permeability of the drop membrane is relatively weak, except in near contact where the lubrication pressure in the narrow gap between the particle and drop surfaces can cause significant permeation of fluid across the membrane, as further described by a lubrication analysis. These results were then used in a trajectory analysis to predict particle collection rates by permeable drops in a dilute suspension undergoing uniaxial extensional (or compressional) flow. Even a small amount of permeation allows for a large increase in the particle collision rate with the drop interface. For example, the collision efficiency (collision rate divided by that in the absence of hydrodynamic interactions) is 0.17 for equisized particles and drops with a dimensionless permeability  $k/a = 0.0001$  (where  $k$  is the membrane permeability per unit thickness, and  $a$  is the reduced radius of the drop and particle). In contrast, it is identically zero (due to the singular lubrication resistance) for smooth, impermeable spheres in the absence of attractive molecular forces and fluid slip.

DOI: [10.1103/PhysRevFluids.3.113601](https://doi.org/10.1103/PhysRevFluids.3.113601)

### I. INTRODUCTION

Aggregation of small solid particles suspended in a liquid is important in various biological (e.g., cell flocculation) and industrial (e.g., coagulation to enhance sedimentation rates) processes. Similarly, droplet coalescence is important in, for example, emulsion processing and raindrop formation. Starting in the 1970s, particle aggregation in dilute suspensions undergoing simple shear or another linear flow and accounting for hydrodynamic interactions was studied by Curtis and Hocking [1], van de Ven and Mason [2], Zeichner and Schowalter [3], and Adler [4], among others. Theoretical analyses of the collision rates of small particles at low Reynolds number are enabled by the formalism of Batchelor and Green [5], who described the general form of the hydrodynamic interaction between a pair of solid spheres in a linear flow field, including asymptotic expressions for large and small separations. A key result is that molecular attractions, such as van der Waals forces, are required to overcome the viscous lubrication resistance and bring the solid spheres into contact (alternatively, a small amount of surface roughness or fluid slip may allow for contact).

Similar analyses of the coalescence of liquid drops suspended in an immiscible fluid were subsequently performed. They account for the internal flow within the drops, as described using the bispherical-coordinate solutions of Zinchenko [6] and Wang, Zinchenko, and Davis [7] for the hydrodynamic interactions between equisized drops and between nonequal drops, respectively, along with the lubrication theory developed by Davis, Schonberg, and Rallison [8] for drops in close approach. The mobility of the drop interfaces weakens the lubrication singularity and allows

---

\*Corresponding author: [robert.davis@colorado.edu](mailto:robert.davis@colorado.edu)

for nonzero collision rates of spherical drops, even in the absence of attractive molecular forces. However, the lubrication pressure in the narrowing gap between the approaching drops eventually becomes large enough to cause deformation of the interfaces, which then prevents collisions without attractive forces or other effects (such as a breakdown of the continuum equations when the gap becomes comparable to the molecular spacing). The effect of slight deformation on drop coalescence with attractive forces was described by Rother and Davis [9].

Of additional interest are particle collisions or collection in heterogeneous systems, such as in the flotation of hydrophobic particles by air bubbles or the scavenging of soot particles from the atmosphere by raindrops or snowflakes. In the present work, we consider the collection of particles in a viscous fluid by droplets covered with thin, permeable membranes. The original motivation for this study is a recent technology described by van Netten, Borrow, and Galvin [10], in which hydrophobic particles are collected from a stirred aqueous suspension by a water-in-oil binder composed of water droplets covered with permeable hydrophobic films. However, we take a fundamental approach that may have applications in other fields, such as ones involving vesicles, cells, or encapsulated liquids. Of relevance is the work of Davis [11], who considered flow due to a porous sphere sedimenting toward a solid sphere or wall, for which a Brinkman-type flow within the particle allows for contact under the action of finite force. Of further relevance is the motion of a solid sphere toward (or away from) a flat, permeable surface, such as encountered during membrane filtration of small particles [12–14]. Permeation of liquid through the membrane allows the particle to collide with (or be removed from) the membrane at a nonzero velocity.

## II. PROBLEM DESCRIPTION AND METHODS

We consider a solid, spherical particle of radius  $a_p$  near a spherical drop of radius  $a_d$ , immersed in a viscous fluid at low Reynolds number,  $\text{Re} = \rho UL/\mu \ll 1$ , and large Péclet number,  $\text{Pe} = UL/D \gg 1$ , where  $\rho$  and  $\mu$  are the fluid density and viscosity,  $U$  is a characteristic flow velocity (e.g., the shear rate times the drop or particle radius),  $D$  the relative Brownian diffusivity, and  $L$  is a characteristic length scale (e.g.,  $a_d$  or  $a_p$ ). For shear rates of  $100 \text{ s}^{-1}$ , drop and particle radii in the approximate range between 1.0 and 100 microns meet these criteria. The particle and drop are assumed force-free and torque-free, so that any gravitational effects are dominated by the imposed flow. The drop is covered by a very thin film or membrane (moving as a rigid body), on which the relative tangential velocity of the fluid is zero but for which the normal relative velocity is proportional to the dynamic pressure drop across the membrane. The constant of proportionality is  $k/\mu$ , where  $k$  is the membrane permeability divided by its thickness (also called the membrane permeance). Typical values of  $k$  for microfiltration membranes are of order  $10^{-4} \mu\text{m}$  [15], so that the dimensionless permeabilities,  $k/a$ , where  $a$  is the reduced radius, are expected to be on the order of  $10^{-4}$ – $10^{-6}$  for reduced radii of 1.0 to 100 microns. Both the particle and drop are assumed to remain spherical, without deformation. The internal fluid of the drop is assumed to have the same viscosity as that of the external fluid, but this assumption is expected to have little bearing on the results, as the permeation and internal flow are typically small. Additionally, the two fluids are assumed essentially isotonic, with any higher osmotic pressure in the external fluid set to just balance any capillary pressure inside the drop due to its interfacial tension. In the method described by van Netten, Borrow, and Galvin [10], salt may be included in the internal phase, which drives osmotic flow across the film into the drops, to enhance particle capture. This possibility is not included in the present work, for which permeation is solely due to the hydrodynamic pressure difference between the external and internal fluids.

Near the particle and drop, the undisturbed external flow is linear in position and thus may be written in the general form

$$\mathbf{U} = \mathbf{U}_0 + \mathbf{E} \cdot \mathbf{x} + \boldsymbol{\Omega} \times \mathbf{x}, \quad (1)$$

where  $\mathbf{U}_0$  is the velocity at the origin and represents uniform flow,  $\mathbf{E}$  is the rate-of-strain tensor and represents pure straining motion, and  $\boldsymbol{\Omega}$  is the rotation vector and represents solid-body rotation. As

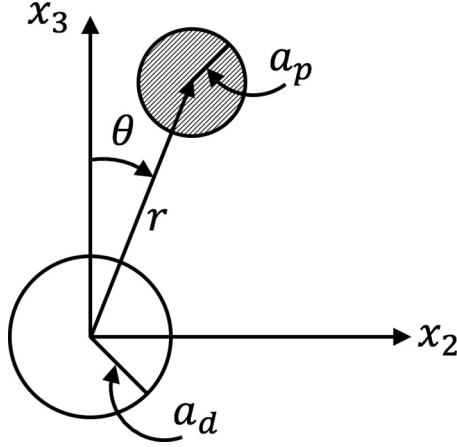


FIG. 1. Coordinate system for the axisymmetric motion of a spherical particle relative to a spherical drop centered at the origin.

described by Batchelor and Green [5], the relative velocity of a particle and drop in this flow field is

$$\mathbf{V}_{pd}(\mathbf{r}) = \boldsymbol{\Omega} \times \mathbf{r} + \mathbf{E} \cdot \mathbf{r} - \left[ A(s) \frac{\mathbf{r}\mathbf{r}}{r^2} + B(s) \left( \mathbf{I} - \frac{\mathbf{r}\mathbf{r}}{r^2} \right) \cdot \mathbf{E} \cdot \mathbf{r} \right], \quad (2)$$

in the absence of attractive or repulsive interactions and with negligible deformation and Brownian motion. Here,  $\mathbf{r}$  is the vector from the center of the drop to the center of the particle (see Fig. 1 for a schematic of the axisymmetric case),  $r = |\mathbf{r}|$ ,  $\mathbf{I}$  is the unit second-order tensor, and  $A(s)$  and  $B(s)$  are two-sphere mobility functions accounting for hydrodynamic interactions along and normal to the line-of-centers, respectively. The mobility functions (see the subsequent section) depend on the dimensionless separation,  $s = 2r/(a_p + a_d)$ , the size ratio  $\lambda = a_p/a_d$ , and the dimensionless permeability,  $K^* = k/a$ , where  $a = a_p a_d / (a_p + a_d)$  is the reduced radius.

Our goal is to calculate the collision efficiency, and show how it depends on the size ratio,  $\lambda$ , and, in particular, the dimensionless permeability,  $K^*$ . The collision efficiency is defined as  $E_{pd} = J_{pd}/J_{pd}^0$ , where  $J_{pd}$  is the collision rate with hydrodynamic interactions and  $J_{pd}^0$  is the collision rate without interactions. For a dilute suspension, in which only pairwise interactions need be considered, the collision rate (# collisions per volume per time) is equal to the flux of particles (#/time) upstream of a drop that pass through a collision cross-section and so collide with the drop, multiplied by the number of drops per volume [7]:

$$J_{pd} = -n_p n_d \int_{A_c} (\boldsymbol{\Omega} \times \mathbf{r} + \mathbf{E} \cdot \mathbf{r}) \cdot \mathbf{n} \, ds, \quad (3)$$

where  $n_p$  and  $n_d$  are the number densities (#/volume) of particles and drops, respectively, and  $A_c$  is an upstream interception surface (far enough from the drop that the particle moves with the undisturbed fluid), with  $\mathbf{n}$  the outward unit normal to the interception surface. All particles passing through the interception area subsequently collide with the drop and are assumed to then adhere and be collected by the drop. In the absence of interactions, the particle follows the undisturbed streamlines and would be collected if the particle center passes within a distance  $a_d + a_p$  of the location of the center of the drop. In what follows, we consider two common linear flows: uniaxial extension/compression and simple shear.

### A. Uniaxial extension/compression

For uniaxial extension or compression,  $\mathbf{U} = (\pm\dot{\gamma}x_1, \pm\dot{\gamma}x_2, \mp 2\dot{\gamma}x_3)$ , with the upper sign for extension and the lower sign for compression, Zeichner and Schowalter [3] showed in the absence

of hydrodynamic interactions that

$$J_{pd}^0 = \frac{8\pi}{3\sqrt{3}} n_p n_d \dot{\gamma} (a_d + a_p)^3. \quad (4)$$

When hydrodynamic interactions are included, a trajectory analysis is performed to determine if a drop and a particle will come into contact. Using uniaxial extension/compression as an example, Eq. (2) may be decomposed into the relative velocity components along and normal to the line-of-centers. Dividing the former by the latter to eliminate time yields,

$$\frac{ds}{d\theta} = -\frac{(1-A)s(3\cos^2\theta - 1)}{3(1-B)\sin\theta\cos\theta}. \quad (5)$$

Note that the solid-body rotation,  $\mathbf{\Omega} \times \mathbf{r}$ , does not play a role in the two-sphere collisions, as it does not change the relative separation distance. Following Wang, Zinchenko, and Davis [7], the trajectory equation may be separated and integrated to yield

$$s^3 \sin^2\theta \cos\theta = C\phi^3(s), \quad (6)$$

where  $C$  is a constant specifying a particular trajectory and

$$\phi(s) = \exp\left[\int_s^\infty \left(\frac{A(s') - B(s')}{1 - A(s')}\right) \frac{ds'}{s'}\right]. \quad (7)$$

Thus, only if  $|C| < C_{\text{cr}} = 16/[3\sqrt{3}\phi^3(2)]$  will the trajectory end in contact or capture, which occurs at  $s = 2$ . The critical trajectories, having  $C = \pm C_{\text{cr}}$ , graze the  $s = 2$  contact surface at  $\theta = \arctan(\sqrt{2})$  and  $\theta = \pi - \arctan(\sqrt{2})$ , as shown in Fig. 2. Then, matching this critical trajectory and constant  $C$  with the streamlines for a value of  $s$  large enough that hydrodynamic interactions may be neglected, allows the collision cross-section (upstream interception surface) to be found. The collision efficiency from Eqs. (3) and (4) is then

$$E_{pd} = J_{pd}/J_{pd}^0 = 1/\phi^3(2). \quad (8)$$

For impermeable, rigid spheres,  $\phi(2) = \infty$ , since  $A(s) \rightarrow 1$  as  $s \rightarrow 2$  due to strong lubrication forces; thus,  $E_{pd} = 0$  for smooth, rigid spheres in the absence of molecular effects and attractive forces. For permeable drops, we expect that the lubrication resistance to close approach of the particle and drop surfaces will be reduced as fluid permeates into the drop, so that  $E_{pd} > 0$ .

## B. Simple Shear

For simple shear flow,  $\mathbf{U} = (\dot{\gamma}x_2, 0, 0)$ , Smoluchowski [16] first showed that

$$J_{pd}^0 = \frac{4}{3} n_p n_d \dot{\gamma} (a_d + a_p)^3, \quad (9)$$

where  $\dot{\gamma}$  is the shear rate.

A trajectory analysis for simple shear flow with hydrodynamic interactions yields [9]

$$E_{pd} = \frac{1}{8} \left[ \frac{4}{\phi^2(2)} - \psi(2) \right], \quad (10)$$

where  $\phi(s)$  is given by Eq. (7) and

$$\psi(s) = \int_s^\infty \frac{B(s')s'ds'}{[1 - A(s')]\phi^2(s')}. \quad (11)$$

As before,  $E_{pd} = 0$  for rigid, impermeable spheres, as  $\phi^2(2)\psi(2) = 4$  in this case [17], again due to strong lubrication interactions. For solid spheres, there are only open trajectories (starting at upstream infinity and ending at downstream infinity) and closed trajectories (in which the two spheres orbit around each other), with no trajectories ending in contact.

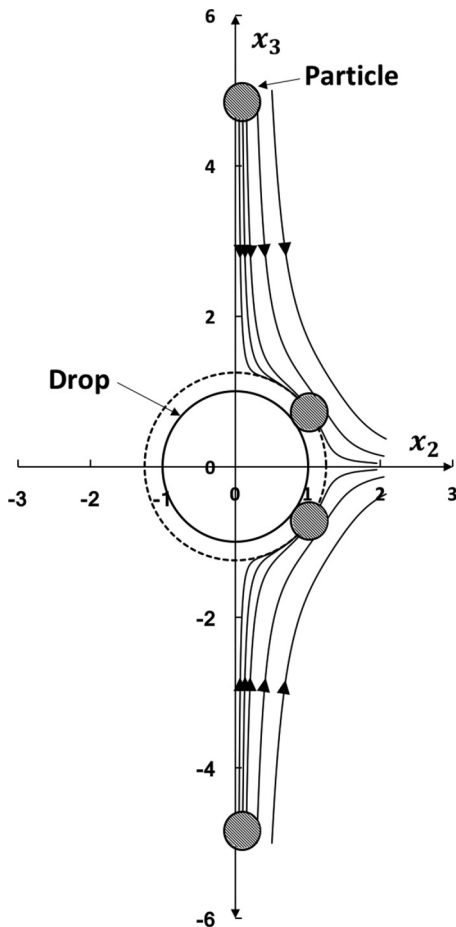


FIG. 2. Example trajectories for  $a_p/a_d = 0.25$  and  $k/a = 0.0001$  in uniaxial extension. The limiting or grazing trajectory is shown with the particle at its ends; only those trajectories inside the limiting trajectory end in contact. The trajectories are symmetric about the  $x_3$  axis, and all lengths are nondimensionalized using the drop radius.

In what follows, mobility functions for a solid particle interacting with a permeable drop are determined, with a particular focus on the near-contact interaction and the reduction in lubrication resistance due to permeation. The resulting mobility functions are then used in Eqs. (7) and (8) or, equivalently, backwards integration of Eq. (5) from the grazing point, to determine the collision efficiency with permeable drops in uniaxial extension or compression.

### III. MOBILITY FUNCTIONS

The mobility functions,  $A(s)$  and  $B(s)$ , quantify the effects of hydrodynamic interactions on the relative motion of two spheres in a linear flow. Following prior work for two solid spheres [5] and two liquid spheres [6,7], arbitrary separations are analyzed using expansions in bispherical coordinates, while the limits of large and small separations are described by the method of reflections and lubrication theory, respectively.

A drop and a particle freely suspended in a linear flow acquire translational velocities  $\mathbf{V}_d$  and  $\mathbf{V}_p$ , respectively, of their centers. The solid particle additionally acquires rigid-body rotation about its center with angular velocity  $\boldsymbol{\omega}_p$ . Likewise, the permeable but rigid membrane covering the spherical

drop surface is in rigid-body motion with angular velocity  $\boldsymbol{\omega}_d$  about the drop center; this rigid-body motion should not be confused with the more complex fluid flow inside the drop. The Reynolds number is assumed small, so that the Stokes equations govern the flow:

$$\nabla \cdot \mathbf{v} = 0, \quad \nabla p = \mu \nabla^2 \mathbf{v}, \quad (12)$$

where  $\mathbf{v}$  is the fluid velocity and  $p$  is the dynamic pressure (with hydrostatic pressure subtracted out). The fluid viscosity  $\mu$  is the same inside and outside the drop, so that Eq. (12) applies for both phases. Far from the drop and particle, the fluid velocity is  $\mathbf{v}(\mathbf{x}) = \mathbf{v}_\infty(\mathbf{x})$ , where  $\mathbf{v}_\infty$  is the imposed far-field flow and  $\mathbf{x}$  is the position vector. On the particle surface, the standard no-slip condition applies:

$$\mathbf{v}(\mathbf{x}) = \mathbf{V}_p + \boldsymbol{\omega}_p \times (\mathbf{x} - \mathbf{x}_p), \quad |\mathbf{x} - \mathbf{x}_p| = a_p, \quad (13)$$

where  $\mathbf{x}_p$  is the instantaneous location of the particle center. On the membrane surface, there is no-slip, plus a normal velocity proportional to the pressure drop:

$$\mathbf{v}(\mathbf{x}) = \mathbf{V}_d + \boldsymbol{\omega}_d \times (\mathbf{x} - \mathbf{x}_d) - \frac{k}{\mu} [p_e(\mathbf{x}) - p_i(\mathbf{x})] \mathbf{n}, \quad |\mathbf{x} - \mathbf{x}_d| = a_d, \quad (14)$$

where the subscripts  $e$  and  $i$  refer to the external and internal fluids, respectively,  $\mathbf{n} = (\mathbf{x} - \mathbf{x}_p)/a_d$  is the outward unit normal, and  $\mathbf{x}_d$  is the instantaneous location of the center of the drop (which, without loss of generality, is set to zero with the drop centered at the origin). Note that Eq. (14) applies to both the internal and external fluid and that the membrane thickness is assumed to be very small compared to the drop radius.

### A. Arbitrary separations

Following the usual approach for two-sphere problems, we first determine the hydrodynamic forces and torques (about the centers) acting on the particle and drop in the resistance formulation, i.e., with prescribed velocities  $\mathbf{V}_p, \mathbf{V}_d, \boldsymbol{\omega}_p, \boldsymbol{\omega}_d$  in a linear flow field  $\mathbf{v}_\infty(\mathbf{x})$ . The zero-force and zero-torque conditions allow us then to relate these velocities to  $\mathbf{v}_\infty(\mathbf{x})$  and hence calculate the mobilities  $A$  and  $B$  in Eq. (2). The resistance coefficients relating forces and torques to prescribed particle/drop kinematics in a quiescent liquid can be also extracted from the solutions below; these coefficients would be essential when describing the particle and drop motion in the presence of external forces (such as gravity or interparticle attraction). However, such generality was not pursued in the present work.

Let  $(x, y, z)$  be a Cartesian coordinate system with the  $z$  axis along the centerline from the drop to the particle; the origin is chosen in the gap region as detailed below. Let  $(\rho, \theta, z)$  be associated cylindrical coordinates ( $x = \rho \cos \theta, y = \rho \sin \theta$ ), with the azimuthal angle  $\theta$  of positive rotation about the  $z$  axis. Determining the mobilities  $A$  and  $B$  is reduced to solving two problems.

*Problem 1.*  $\mathbf{v}_\infty(\mathbf{x}) = (-E_{33}x/2, -E_{33}y/2, E_{33}z)$ . Under the action of this axisymmetrical straining flow, the particle and drop centers acquire the velocities  $(0, 0, V_p)$  and  $(0, 0, V_d)$ . The solution using (2) gives  $A = 1 - (V_p - V_d)/(rE_{33})$ .

*Problem 2.*  $\mathbf{v}_\infty(\mathbf{x}) = (Gz, 0, 0)$ . In this simple shear flow, the particle and drop centers acquire the velocities  $(V_p, 0, 0)$  and  $(V_d, 0, 0)$ . This flow also generates the rotational velocities  $(0, \omega_p, 0)$  and  $(0, \omega_d, 0)$  for the particle and drop membrane motion about the centers. The solution using Eq. (2) gives  $B = 2[1 - (V_p - V_d)/(Gr)]$ .

Both problems are solved in bispherical coordinates  $\xi, \eta$  introduced as follows:

$$z = \frac{c \sinh \eta}{\cosh \eta - v}, \quad \rho = \frac{c \sin \xi}{\cosh \eta - v}, \quad v = \cos \xi, \quad 0 < \xi \leq \pi, \quad -\infty < \eta < \infty. \quad (15)$$

The particle and drop shapes become coordinate surfaces  $\eta = \eta_p$  and  $\eta = \eta_d$ , respectively, if the parameters  $\eta_p > 0, \eta_d < 0$  and  $c > 0$  are determined from the relations

$$r = a_p \cosh \eta_p + a_d \cosh \eta_d, \quad |\sinh \eta_d| = \lambda \sinh \eta_p, \quad c = a_p \sinh \eta_p = a_d |\sinh \eta_d| \quad (16)$$

(see Wang, Zinchenko, and Davis [7] for explicit expressions).

*Solution of Problem 1.* For this axisymmetrical case, the stream-function approach of Goren [12] could be potentially used. However, in his work on the solid sphere motion toward/away from a plane porous membrane in a quiescent liquid, many simplifications arose in the bispherical-coordinate solution due to  $\eta = 0$  on the permeable surface. Accordingly, his problem could be reduced to a single, fourth-order difference equation for the coefficients in the series expansion. Due to  $\eta_d \neq 0$ , the stream-function approach would be much harder to apply in the present work. Instead, a more straightforward (but still efficient) flow representation in primitive variables (velocity-pressure) is chosen herein, based on the general Stokes flow series solution in bispherical coordinates derived by Lin, Lee, and Sather [18]. As follows from their work, the axisymmetrical form for the velocity components  $v_\rho$ ,  $v_z$  and pressure  $p$  between the spheres ( $\eta_d < \eta < \eta_p$ ) and inside the drop ( $\eta < \eta_p$ ) can be sought as

$$v_\rho = \frac{\rho}{c}F + \Phi, \quad v_z = \frac{z}{c}F + \Psi, \quad p = \mu \frac{2F}{c}, \quad (17)$$

with series expansions

$$F = \zeta \sum_{n=0}^{\infty} f_n(\eta)P_n(v), \quad \Phi = \zeta \sum_{n=1}^{\infty} \varphi_n(\eta) \sin \xi P'_n(v), \quad \Psi = \zeta \sum_{n=0}^{\infty} \psi_n(\eta)P_n(v). \quad (18)$$

Here,  $\zeta = (\cosh \eta - v)^{1/2}$  and  $P_n(v)$  is the Legendre polynomial of degree  $n$ . In the region between the spheres (marked by index  $e$  in what follows),

$$\begin{aligned} \varphi_n^e(\eta) &= A_n^e \exp[(n+1/2)(\eta - \eta_p)] + B_n^e \exp[(n+1/2)(\eta_d - \eta)] + \varphi_n^\infty(\eta), \\ f_n^e(\eta) &= C_n^e \exp[(n+1/2)(\eta - \eta_p)] + D_n^e \exp[(n+1/2)(\eta_d - \eta)], \\ \psi_n^e(\eta) &= E_n^e \exp[(n+1/2)(\eta - \eta_p)] + F_n^e \exp[(n+1/2)(\eta_d - \eta)] + \psi_n^\infty(\eta), \end{aligned} \quad (19)$$

where  $A_n^e \dots F_n^e$  are unknown coefficients, and

$$\begin{aligned} \varphi_n^\infty(\eta) &= -E_{33}c\sqrt{2} \exp[-(n+1/2)|\eta|], \\ \psi_n^\infty(\eta) &= \pm E_{33}c\sqrt{2}(2n+1) \exp[-(n+1/2)|\eta|]. \end{aligned} \quad (20)$$

The terms with  $\eta_p$  and  $\eta_d$  are introduced into Eq. (16) for normalization purposes. The upper sign in Eq. (20) applies for  $\eta > 0$ , the lower sign for  $\eta < 0$ . The contribution of  $\varphi_n^\infty(\eta)$  and  $\psi_n^\infty(\eta)$  to the fluid velocities Eq. (17) is to produce the unperturbed flow field  $\mathbf{v}_\infty(\mathbf{x})$ ; the additional contribution due to the coefficients  $A_n^e \dots F_n^e$  generates the velocity perturbation vanishing at  $\mathbf{x} \rightarrow \infty$ .

Because of the bispherical-coordinate singularity  $\eta = -\infty$  inside the drop (at the pole  $z = -c$ ,  $\rho = 0$ ), only the terms proportional to  $\exp[(n+1/2)\eta]$  are left in the expressions for the internal flow field:

$$\begin{aligned} \varphi_n^i(\eta) &= A_n^i \exp[(n+1/2)(\eta - \eta_p)] + \varphi_n^\infty(\eta), \\ f_n^i(\eta) &= C_n^i \exp[(n+1/2)(\eta - \eta_p)], \\ \psi_n^i(\eta) &= E_n^i \exp[(n+1/2)(\eta - \eta_p)] + \psi_n^\infty(\eta), \end{aligned} \quad (21)$$

with unknown coefficients  $A_n^i$ ,  $C_n^i$  and  $E_n^i$ ; index  $i$  marks the values for the flow inside the drop. Equations (17)–(21) produce flows automatically satisfying the Stokes equation  $\mu \nabla^2 \mathbf{v} = \nabla p$ , but the continuity equation  $\nabla \cdot \mathbf{v} = 0$  between the spheres and inside the drop requires

$$\begin{aligned} 5C_n^e - ne^{\eta_p}C_{n-1}^e + (n+1)e^{-\eta_p}C_{n+1}^e + n(n-1)e^{\eta_p}A_{n-1}^e + (n+1)(n+2)e^{-\eta_p}A_{n+1}^e \\ - 2n(n+1)A_n^e + (2n+1)E_n^e - ne^{\eta_p}E_{n-1}^e - (n+1)e^{-\eta_p}E_{n+1}^e = 0, \end{aligned} \quad (22)$$

$$\begin{aligned} 5D_n^e - ne^{-\eta_d}D_{n-1}^e + (n+1)e^{\eta_d}D_{n+1}^e + n(n-1)e^{-\eta_d}B_{n-1}^e + (n+1)(n+2)e^{\eta_d}B_{n+1}^e \\ - 2n(n+1)B_n^e - (2n+1)F_n^e + ne^{-\eta_d}F_{n-1}^e + (n+1)e^{\eta_d}F_{n+1}^e = 0, \end{aligned} \quad (23)$$

$$\begin{aligned}
 5C_n^i - ne^{\eta p} C_{n-1}^i + (n+1)e^{-\eta p} C_{n+1}^i + n(n-1)e^{\eta p} A_{n-1}^i + (n+1)(n+2)e^{-\eta p} A_{n+1}^i \\
 - 2n(n+1)A_n^i + (2n+1)E_n^i - ne^{\eta p} E_{n-1}^i - (n+1)e^{-\eta p} E_{n+1}^i = 0,
 \end{aligned} \quad (24)$$

for all  $n \geq 0$ .

Using recurrent relations between Legendre functions, the fluid velocity continuity  $\mathbf{v}^e = \mathbf{v}^i$  on the drop surface yields

$$\varphi_n^i(\eta_d) - \varphi_n^e(\eta_d) = \frac{1}{\sinh \eta_d} \left( \frac{Z_{n-1}}{2n-1} - \frac{Z_{n+1}}{2n+3} \right), \quad n \geq 1, \quad (25)$$

and

$$\Delta f_n = \frac{1}{\sinh \eta_d} \left[ \frac{nZ_{n-1}}{2n-1} + \frac{(n+1)Z_{n+1}}{2n+3} - Z_n \cosh \eta_d \right], \quad n \geq 0, \quad (26)$$

where, for brevity,

$$Z_n = \psi_n^i(\eta_d) - \psi_n^e(\eta_d), \quad \Delta f_n = f_n^i(\eta_d) - f_n^e(\eta_d). \quad (27)$$

Based on Eqs. (19), (21), and (25)–(27), the internal coefficients  $A_n^i$ ,  $C_n^i$ ,  $E_n^i$  can be expressed via the external  $A_n^e \dots F_n^e$  coefficients and  $Z_m$  ( $n-1 \leq m \leq n+1$ ). Substituting such expressions into Eq. (24) and combining the result with Eq. (22) replaces the continuity equation for the internal flow by a more manageable form:

$$\begin{aligned}
 5D_n^e - ne^{\eta d} D_{n-1}^e + (n+1)e^{-\eta d} D_{n+1}^e + n(n-1)e^{\eta d} B_{n-1}^e + (n+1)(n+2)e^{-\eta d} B_{n+1}^e \\
 - 2n(n+1)B_n^e + (2n+1)F_n^e - ne^{\eta d} F_{n-1}^e - (n+1)e^{-\eta d} F_{n+1}^e \\
 + \frac{2}{\sinh \eta_d} \left[ \frac{nZ_{n-1}}{2n-1} + \frac{(n+1)Z_{n+1}}{2n+3} - \left( \cosh \eta_d + \frac{\sinh \eta_d}{2n+1} \right) Z_n \right] = 0,
 \end{aligned} \quad (28)$$

where the internal flow coefficients are present only through  $Z_m$ .

To implement the remaining boundary conditions on the drop surface, consider the relative fluid velocity  $\tilde{\mathbf{v}}^d = \mathbf{v}^e - \mathbf{V}_d$  of the carrier fluid near the sphere  $\eta = \eta_d$ . This velocity is still represented by Eqs. (17)–(20), with  $\psi_n^e(\eta)$  replaced by

$$\tilde{\psi}_n^d(\eta) = \psi_n^e(\eta) - V_d \sqrt{2} \exp[(n+1/2)\eta]. \quad (29)$$

The boundary condition of zero tangential relative velocity  $\tilde{v}_\xi^d = 0$  yields

$$\begin{aligned}
 \frac{f_{n+1}^e \cosh \eta + \tilde{\psi}_{n+1}^d \sinh \eta}{2n+3} - \frac{f_{n-1}^e \cosh \eta + \tilde{\psi}_{n-1}^d \sinh \eta}{2n-1} \\
 + \cosh \eta \left[ \frac{(n-1)\varphi_{n-1}^e}{2n-1} + \frac{(n+2)\varphi_{n+1}^e}{2n+3} \right] - \varphi_n^e = 0,
 \end{aligned} \quad (30)$$

at  $\eta = \eta_d$ ,  $n \geq 1$ .

The final boundary condition on the drop surface connects the relative normal fluid velocity in the outward normal direction to the pressure jump across the interface, which can be written as  $\tilde{v}_\eta^d = 2\gamma[F^i - F^e]$  (with  $\gamma = k/c$ ). After some algebra using Eqs. (15), (17), and (18) and recurrent

relations between Legendre functions, this condition results in

$$\begin{aligned} & \tilde{\psi}_n^d - \frac{n}{2n-1} [f_{n-1}^e \sinh \eta + \tilde{\psi}_{n-1}^d \cosh \eta] - \frac{n+1}{2n+3} [f_{n+1}^e \sinh \eta + \tilde{\psi}_{n+1}^d \cosh \eta] \\ & + \sinh \eta \left[ \frac{n(n-1)\varphi_{n-1}^e}{2n-1} - \frac{(n+1)(n+2)\varphi_{n+1}^e}{2n+3} \right] \\ & = 2\gamma \left[ \Delta f_n \cosh \eta - \frac{n}{2n-1} \Delta f_{n-1} - \frac{n+1}{2n+3} \Delta f_{n+1} \right] \end{aligned} \quad (31)$$

at  $\eta = \eta_d$ ,  $n \geq 0$ .

Near the solid particle surface  $\eta = \eta_p$ , it is again convenient to introduce the relative fluid velocity  $\tilde{\mathbf{v}}^p = \mathbf{v}^e - V_p$ . This velocity is still represented by Eqs. (17)–(20), with  $\psi_n^e(\eta)$  replaced by

$$\tilde{\psi}_n^p(\eta) = \psi_n^e(\eta) - V_p \sqrt{2} \exp[-(n+1/2)\eta]. \quad (32)$$

The no-slip boundary condition  $\tilde{\mathbf{v}}^p = \mathbf{0}$  yields two final equations:

$$\varphi_n^e + \frac{1}{\sinh \eta} \left( \frac{\tilde{\psi}_{n+1}^p}{2n+3} - \frac{\tilde{\psi}_{n-1}^p}{2n-1} \right) = 0 \quad \text{at } \eta = \eta_p, \quad n \geq 1 \quad (33)$$

and

$$f_n^e + \frac{1}{\sinh \eta} \left[ \tilde{\psi}_n^p \cosh \eta - \frac{n\tilde{\psi}_{n-1}^p}{2n-1} - \frac{(n+1)\tilde{\psi}_{n+1}^p}{2n+3} \right] = 0 \quad \text{at } \eta = \eta_p, \quad n \geq 0. \quad (34)$$

Relations Eqs. (22), (23), (26), (28), (30), (32), (33), and (34), complemented by the definitions Eqs. (19), (20), (29), and (32), present a compact form of eight difference equations for the solution vector  $\mathbf{X}_n = (A_n^e, B_n^e, C_n^e, D_n^e, E_n^e, F_n^e, Z_n, \Delta f_n)$ . Moving the inhomogeneous terms to the right-hand side, these equations can be written in a general form as

$$\alpha_n \mathbf{X}_{n-1} + \beta_n \mathbf{X}_{n+1} + \gamma_n \mathbf{X}_{n+1} = V_p \mathbf{g}_n^1 + V_d \mathbf{g}_n^2 + E_{33} \mathbf{g}_n^3, \quad (35)$$

for  $n \geq 1$ ; the vectors  $\mathbf{g}_n^1$ ,  $\mathbf{g}_n^2$ ,  $\mathbf{g}_n^3$  represent three different cases when the flow is due to particle/drop translation in a quiescent liquid, or due to the ambient flow with the drop and particle at rest. At  $n = 0$ , Eqs. (30) and (33) are not applicable and are replaced by  $B_0^e = 0$  and  $A_0^e = 0$ , respectively, which extends the system (35) to  $n = 0$ , thus allowing one to start the forward sweep of the Thomas algorithm for Eq. (35). The regularity condition  $\mathbf{X}_n \rightarrow 0$  (at  $n \rightarrow \infty$ ) then selects the unique solution of Eq. (35) by backward substitutions.

The hydrodynamic forces acting on the particle ( $F_p$ ) and drop ( $F_d$ ) along the  $z$  axis are

$$F_p = -8\pi \mu c \sqrt{2} \sum_{n=0}^{\infty} E_n^e \exp[-(n+1/2)\eta_p], \quad F_d = -8\pi \mu c \sqrt{2} \sum_{n=0}^{\infty} F_n^e \exp[(n+1/2)\eta_d]. \quad (36)$$

It is very convenient that the forces Eq. (36) can be computed without knowing the solution vector  $\mathbf{X}_n$ . Namely, the forward sweep for system Eq. (35) from  $n = 0$  allows us to express the partial sums (35) to  $n = N$  as  $\mathbf{Q}_N \mathbf{X}_N + \mathbf{R}_N$ , with recurrent calculation of matrices  $\mathbf{Q}_N$  and vectors  $\mathbf{R}_N$ . As  $N \rightarrow \infty$ ,  $\mathbf{Q}_N \mathbf{X}_N$  does not contribute, and so the forces are simply computed as  $\lim_{N \rightarrow \infty} \mathbf{R}_N$ . This approach (first used by Zinchenko [19]) also provides automatic convergence control for bispherical-coordinate series solutions, which is especially beneficial at small surface separations when many terms in the series may be required.

When  $k = 0$ , the present algorithm has been tested at arbitrary separations, with perfect agreement, against known bispherical-coordinate solutions for two impermeable spheres moving along the line-of-centers, including calculation of the resistance coefficients (Cooley and O'Neill [20]) and the  $A(s)$ -mobility function (Lin, Lee, and Sather [18]). For finite drop permeabilities and

TABLE I. Stokes drag correction factor for a solid particle approaching a porous membrane-covered drop along the line of centers for  $k/a_p = 0.1$  and extreme size ratios  $\lambda = a_p/a_d$ .

$h/a_p$	$\lambda = 0.1$	$\lambda = 0.01$	$\lambda = 0.001$	$\lambda = 0$ [12]
2	1.420	1.488	1.496	1.496
1	1.768	1.851	1.860	1.859
0.5	2.213	2.296	2.305	2.302
0.1	2.853	2.895	2.900	2.890

the drop-particle distance  $r \rightarrow \infty$ , perfect agreement was observed with the analytical formula for the hydrodynamical force on an isolated drop:

$$F_d = -6\pi\mu a_d V_d \frac{10(k/a_d) + 1}{10.5(k/a_d) + 1}. \quad (37)$$

The force on a solid particle moving towards a planar permeable membrane with a prescribed velocity (the problem solved by Goren [12]) can be also approached by the present algorithm as an extreme case when the size ratio  $\lambda = a_p/a_d \rightarrow 0$  with fixed surface clearance  $h$  relative to  $a_p$  and fixed  $k/a_p$ . In Table I, the correction factor to Stokes drag is shown for  $k/a_p = 0.1$  (corresponding to Goren's parameter  $\gamma r = 10$ ), different values of  $h/a_p$ , and several small values of  $\lambda$ . The results for  $\lambda = 0.1, 0.01$ , and  $0.001$  were obtained in the present work; the  $\lambda = 0$  data are from Goren [12]; as  $\lambda \rightarrow 0$ , excellent agreement is observed. The present algorithm is not directly applicable at  $\lambda = 0$  and would eventually become ill-conditioned in this limit.

Excellent agreement was also observed between our numerical values of the mobility function  $A(s)$  and the far-field asymptotic form (see Eq. (42) below) when  $s \rightarrow \infty$ ; surface separation of just a few particle/drop radii is sufficient to make Eq. (42) a very accurate approximation.

*Solution of Problem 2.* For this nonaxisymmetrical problem, our bispherical-coordinate solution is based on Dean-O'Neill's flow representation (which was widely used in prior work to handle two particle motions/rotations normal to the centerline [21]):

$$v_\rho = \left(\frac{\rho}{c}F + \chi + \psi\right) \cos \theta, \quad v_\theta = (\chi - \psi) \sin \theta, \quad v_z = \left(\frac{z}{c}F + 2\Phi\right) \cos \theta, \quad p = \mu \frac{2F}{c} \cos \theta, \quad (38)$$

with the series expansions

$$\begin{aligned} F &= \zeta \sum_{n=1}^{\infty} f_n(\eta) P_n^1(v), & \Phi &= \zeta \sum_{n=1}^{\infty} \varphi_n(\eta) P_n^1(v), \\ \psi &= \zeta \sum_{n=0}^{\infty} \psi_n(\eta) P_n(v), & \chi &= \zeta \sum_{n=2}^{\infty} \chi_n(\eta) P_n^2(v). \end{aligned} \quad (39)$$

Here,  $P_n^m(v) = (1 - v^2)^{m/2} d^m P_n(v) / dv^m$  is the associated Legendre function. The expressions for  $f_n(\eta)$ ,  $\varphi_n(\eta)$ ,  $\psi_n(\eta)$  and  $\chi_n(\eta)$  between the spheres and inside the drop are analogous to those in Eqs. (16) and (18) with new coefficients  $A_n$ ,  $B_n$  etc., and ambient-flow representation slightly different from Eq. (17). Additional  $G_n$  and  $H_n$  coefficients represent the  $\chi$ -functions. The continuity equations between the spheres and inside the drop, and boundary conditions on the drop and particle surfaces are reduced to the tridiagonal system of equations of the type Eq. (32) for an extended solution vector  $\mathbf{X}_n$  (which now includes ten unknown sequences of coefficients). The details are cumbersome and outlined in the Appendix. As in the solution of Problem 1, the hydrodynamical forces and torques are conveniently computed as convergent recurrent sequences (at  $N \rightarrow \infty$ ) generated on the forward sweep of the Thomas algorithm; backward substitutions to obtain  $\mathbf{X}_n$  are not required.

In Problem 2, the effect of drop membrane permeability on the mobility  $B$  (and underlying resistance coefficients) was found to be quite weak, even at small surface separations. This result is most likely due to assumed high anisotropy of the porous membrane material covering the drop surface, which allows filtration in the normal direction only and has no slip in the tangential direction.

### B. Far-field expressions

In the case of two solid spheres, far-field expressions for the mobility functions  $A$  and  $B$  were derived by Batchelor and Green [5], based on the solution for a single sphere freely suspended in a linear flow, and the Faxen law. The present case, however, is more difficult for far-field analysis. First, the pressure and velocity disturbances due to a single drop of radius  $a_d$  covered with a permeable membrane have more complex forms:

$$p(\mathbf{r}) = -5\kappa a_d^3 \frac{\mathbf{n} \cdot \mathbf{E} \cdot \mathbf{n}}{r^3} \quad (40)$$

and

$$\hat{\mathbf{u}}(\mathbf{r}) = -\frac{5}{2}\kappa a_d^3 \frac{(\mathbf{n} \cdot \mathbf{E} \cdot \mathbf{n})\mathbf{n}}{r^2} + \frac{a_d^5}{r^4} \left[ -\mathbf{E} \cdot \mathbf{n} + \frac{5}{2}(\mathbf{n} \cdot \mathbf{E} \cdot \mathbf{n})\mathbf{n} \right], \quad (41)$$

as for impermeable spheres, where  $\mathbf{r}$  is the radius vector from the sphere center to the observation point,  $\mathbf{n} = \mathbf{r}/r$ , but with the introduction of an additional parameter:

$$\kappa = \frac{21(k/a_d) + 2}{25(k/a_d) + 2} = \frac{21\lambda K^*/(1 + \lambda) + 2}{25\lambda K^*/(1 + \lambda) + 2}. \quad (42)$$

Second, the classical Faxen law for a solid sphere freely suspended in an unbounded (generally, nonlinear) Stokes flow is not applicable to a drop covered by a porous membrane and must be replaced by

$$\mathbf{U} = \mathbf{u}_0 + \frac{1}{6}a_d^2\eta(\nabla^2\mathbf{u})_0, \quad (43)$$

with

$$\eta = \frac{12(k/a_d) + 1}{10(k/a_d) + 1} = \frac{12\lambda K^*/(1 + \lambda) + 1}{10\lambda K^*/(1 + \lambda) + 1}. \quad (44)$$

Here,  $\mathbf{U}$  is the drop center velocity acquired in the ambient flow  $\mathbf{u}$ ; index 0 denotes the values of  $\mathbf{u}$  and its Laplacian calculated at the drop center, in the absence of the drop. A straightforward (although lengthy) way to derive Eqs. (37)–(41) is to use Lamb's general form for Stokes flow solutions outside and inside the drop.

In other respects, derivation of far-field forms for the mobility functions follows Batchelor and Green [5], resulting in

$$A = 20 \frac{(\kappa + \lambda^3) \frac{1}{s^3}}{(1 + \lambda)^3} - \frac{16[3(1 + \lambda^5) + 5\lambda^2(\kappa + \lambda\eta)] \frac{1}{s^5}}{(1 + \lambda)^5} + \mathcal{O}\left(\frac{1}{s^6}\right) \quad (45)$$

and

$$B = \frac{32[1 + \lambda^5 + 5\lambda^2(\kappa + \lambda\eta)/3] \frac{1}{s^5}}{(1 + \lambda)^5} + \mathcal{O}\left(\frac{1}{s^8}\right). \quad (46)$$

For an impermeable drop ( $K^* = 0$ ,  $\kappa = \eta = 1$ ), Eqs. (42) and (43) agree with Batchelor and Green [5].

### C. Near-field expressions

When the two spheres are in close contact, lubrication theory may be used to determine the relative mobility function along the line-of-centers,  $A(s)$ , except for moderate and large values of  $K^*$ , when the lubrication resistance becomes too small due to permeation. When in near contact, the two spheres are pushed together by the imposed linear flow and experience a contact force [9]. For uniaxial extensional flow, the component of the contact force acting along the line-of-centers is [9]

$$F_c = -6\pi\mu a^2\dot{\gamma}\frac{(1+\lambda)^2}{\lambda}C_1(3\cos^2\theta - 1), \quad (47)$$

where  $C_1$  is the limiting value of  $(1 - A(s))/G(s)$  as  $s \rightarrow 2$ , and  $G(s)$  is the mobility function along the line-of-centers under the action of an equal and opposite force on the two spheres, as defined by Batchelor and Green [5]. The sign is reversed for compressional flow, and a similar expression holds for shear flow - except the angular dependence on the right-hand-side of Eq. (47) is modified [9]. Note that the constant  $C_1 = [1 - A(s)]/G(s)$  in the contact limit  $s \rightarrow 2$  has an  $O(1)$  value, even though both  $1 - A$  and  $G \rightarrow 0$  in this limit for rigid spheres.

The contact force pushing the spheres together is balanced by a lubrication force resisting their relative approach:

$$F_L = 6\pi\mu a^2 V_{pd} f(\text{Pm})/h_0, \quad (48)$$

where  $V_{pd}$  is the relative velocity of the particle toward the drop along the line-of-centers,  $h_0$  is the gap thickness separating the surfaces of the drop and particle at their noses (i.e., at the line-of-centers), and  $\text{Pm} = ak/h_0^2 = K^*(a/h_0)^2$  is a modified dimensionless permeability. The function  $f(\text{Pm})$  is the ratio of the lubrication force with permeation to that for solid spheres without permeation. It becomes unity as  $\text{Pm} \rightarrow 0$  (rigid, impermeable spheres) and tends to zero as  $\text{Pm} \rightarrow \infty$  (large permeation), as described below. Balancing the two forces yields

$$V_{pd} = \frac{h_0\dot{\gamma}(1+\lambda)^2}{\lambda f(\text{Pm})}C_1(3\cos^2\theta - 1). \quad (49)$$

Then, using Eq. (2) for the relative velocity and taking the component *inward* along the line-of-centers,

$$V_{pd} = -\mathbf{V}_{pd} \cdot \mathbf{r}/r = [1 - A(s)](\mathbf{r}/r) \cdot \mathbf{E} \cdot \mathbf{r}. \quad (50)$$

Noting that  $\mathbf{E} \cdot \mathbf{r} = (\dot{\gamma}x_1, \dot{\gamma}x_2, -2\dot{\gamma}x_3)$  for uniaxial extension, and setting  $r \approx a_d + a_p$  for near contact, equating these two expressions for  $V_{pd}$  then yields

$$1 - A(s) = \frac{C_1(s-2)(1+\lambda)^2}{2\lambda f(\text{Pm})} \quad (51)$$

for  $s - 2 \ll 1$ . An identical result is achieved for shear flow and more general linear flows. However, this analysis applies only for  $K^* \ll 1$ , since larger values of  $K^*$  allow for the imposed flow to push the spheres together without a lubrication resistance. This feature is further discussed and quantified later in the paper.

Lubrication theory for the similar problem of a sphere moving toward (or away from) a flat, permeable membrane under the action of a finite force was described by Ramon *et al.* [14]. Here, we outline the approach for the present problem with a goal of determining the dimensionless lubrication force function,  $f(\text{Pm})$ , and showing how it may be deduced from the results of Ramon *et al.* [14]. A close-up of the lubrication region is shown schematically in Fig. 3. The spherical surfaces of the particle and drop may be approximated by paraboloids in the region of near contact:

$$z_p = h_0 + r^2/2a_p, \quad z_d = -r^2/2a_d, \quad (52)$$

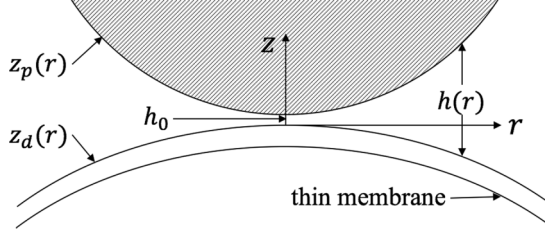


FIG. 3. Schematic of the lubrication region of close contact between a particle and a membrane-covered drop.

where  $h_0$  is the minimum separation and it is assumed that neither surface is deformed by the lubrication pressure. Then, the gap profile is

$$h(r, t) = z_p - z_d = h_0 + r^2/2a, \quad (53)$$

with  $a = a_p a_d / (a_p + a_d)$  the reduced radius.

When  $\rho V_{pd} h_0 / \mu \ll 1$  and  $h_0 / a \ll 1$ , the radial component of the Navier-Stokes equation reduces to

$$\frac{\partial^2 v_r}{\partial z^2} = \frac{1}{\mu} \frac{dp}{dr}, \quad (54)$$

which can be integrated twice to give locally parabolic flow:

$$v_r(r, z) = \frac{1}{2\mu} \frac{dp}{dr} (z - z_p)(z - z_d), \quad (55)$$

using the boundary conditions of no tangential velocity on both surfaces and noting that the dynamic pressure is a function of  $r$  but not  $z$  from the axial component of the Navier-Stokes equation. The equation of continuity is then integrated across the gap to yield

$$V_{pd} - \frac{k}{\mu} p = -\frac{1}{12\mu r} \frac{d}{dr} \left[ r h^3 \frac{dp_d}{dr} \right], \quad (56)$$

using the boundary conditions  $V_z = -V_{pd}$  on the particle surface and  $V_z = -kp/\mu$  on the drop surface (it is presumed that  $p \approx 0$  inside the drop, as the flow is relatively weak inside) for  $K^* \ll 1$ .

The appropriate length scales are  $h_0$  and  $\sqrt{ah_0}$  in the axial and radial directions, respectively, and the pressure scale is  $\mu a V_{pd} / h_0^2$ . Equation (54) is then nondimensionalized using these scales, resulting in an equation equivalent to that given by Ramon *et al.* [14] and containing the dimensionless permeability  $\text{Pm} = ak/h_0^2$ , where  $\text{Pm} = \beta/24$  from their notation. For  $\text{Pm} \ll 1$ , as may be expected during the initial stages of close approach when  $h_0$  is not so small and permeation is weak ( $kp_d/\mu \ll V_{pd}$ ), yielding the classical solution for solid spheres:

$$p_d^0(r) = 3\mu a V_{pd} / (h_0 + r^2/2a)^2 \quad \text{for } \text{Pm} \rightarrow 0. \quad (57)$$

This result may be integrated over the lubrication area to give the lubrication force

$$F_L^0 = 2\pi \int_0^\infty p_d^0(r) r dr = 6\pi \mu a^2 V_{pd} / h_0, \quad (58)$$

where the upper limit of  $r = O(a)$  is replaced by  $\infty$ , since  $r$  scales as  $\sqrt{ah_0}$  in the gap and  $p_d(r)$  decays to zero for  $r \gg \sqrt{ah_0}$ . The superscript "0" in Eqs. (57) and (58) refers to the leading-order solution for impermeable, solid spheres. Ramon *et al.* [14] showed that a series solution with additional terms may be found for small modified permeability:

$$f(\text{Pm}) = 1 - \text{Pm} + \frac{3}{2}\text{Pm}^2 + O(\text{Pm}^3), \quad \text{Pm} \ll 1, \quad (59)$$

where  $f(\text{Pm}) = F_L(\text{Pm})/F_L^0$  and the lubrication pressure with permeation is

$$F_L \approx 2\pi \int_0^\infty p_d(r) r dr, \quad (60)$$

with  $p_d(r)$  the numerical or asymptotic solution of Eq. (56).

In the opposite limit of  $\text{Pm} \gg 1$ , as would be expected as contact is approached, the permeation is large and so the pressure is relatively small, scaling as  $p_d \sim \mu V_{pd}/k \rightarrow 0$  as  $\text{Pm} \rightarrow \infty$ . A matched-asymptotic expansion is then needed to determine the form of  $p_d(r)$  for small but nonzero  $\text{Pm}^{-1} = h_0^2/(ak)$  and, hence, the lubrication force [14]:

$$f(\text{Pm}) = \sqrt{\frac{2}{3}} \text{Pm}^{-1/2} - \frac{1}{4} \text{Pm}^{-1} + \frac{\sqrt{3}}{96\sqrt{2}} \text{Pm}^{-3/2} + O(\text{Pm}^{-2}), \quad \text{Pm} \gg 1. \quad (61)$$

The leading term, which dominates in the limit of the solid sphere touching the membrane, was also found numerically by Goren [12] and verified by Nir [13]. Of practical significance is that the lubrication force remains finite as contact occurs, so that the spheres make contact with a finite velocity due to the permeation. Combining Eq. (48) with the leading term of Eq. (61), along with the definition  $\text{Pm} = K^*(a/h_0)^2$ , gives

$$F_L = 6\pi\mu a V_{pd} \left( \frac{2}{3K^*} \right)^{1/2} \quad \text{as } h_0/a \rightarrow 0. \quad (62)$$

Of particular interest for the current application, the relative mobility along the line-of-centers from Eq. (48) becomes

$$1 - A(s) = C_1(3K^*/2)^{1/2} \quad \text{for } s \rightarrow 2, \quad (63)$$

thus reaching a constant value (albeit small for typical  $K^* \ll 1$ ) as contact is approached. It is anticipated that these expressions will be accurate only for  $K^* \leq O(10^{-3})$ , so that  $(2/(3K^*))^{-1/2} \gg 1$  and there is an appreciable lubrication resistance to the hydrodynamic forces acting on the rest of the sphere surfaces to push them together.

The mobility function for relative motion normal to the line-of-centers,  $B(s)$ , approaches a nonzero constant of  $O(1)$  as the spheres touch, even in the absence of permeation. The rate of approach to this constant as the gap becomes small is slow [5]:

$$B(s) \sim B_0 + \frac{B_1}{\ln[1/(s-2)]} + O\left(\frac{1}{\{\ln[1/(s-2)]\}^2}\right). \quad (64)$$

The constants  $B_0$  and  $B_1$  are functions of the size ratio,  $\lambda = a_p/a_d$ . As seen in the Results and Discussion section, they are also weak functions of the dimensionless permeability,  $K^* = k/a$ .

## IV. RESULTS AND DISCUSSION

### A. Mobility Functions

Figure 4 shows the relative mobility function along the line-of-centers, plotted as  $1 - A(s)$  versus the dimensionless separation  $s - 2$  for size ratios  $\lambda = 1$  and  $1/2$  and several values of the dimensionless permeability. A log-log plot is used to emphasize the behavior at small separations. Note that  $1 - A(s)$  is the dimensionless relative velocity of the two spheres toward each other, with  $A(s)$  accounting for the hydrodynamic interactions that reduce the relative velocity from that of the undisturbed flow. For  $s - 2 \gtrsim 1$ , the far-field expression given by Eq. (45) is an accurate representation of the numerical results, and there is only a small effect of permeation. The effect of permeation on the mobility remains small for separations  $s - 2 \gtrsim 3(K^*)^{1/2}$ , with  $K^* \ll 1$ .

When  $s - 2 \lesssim 3(K^*)^{1/2}$ , permeation becomes important. The  $1 - A$  values for  $K^* > 0$  then level out and reach a constant value  $1 - A_0$  as the dimensionless gap,  $s - 2$ , becomes small, in contrast to the impermeable case,  $K^* = 0$ , for which  $1 - A$  continues to decrease in proportion to

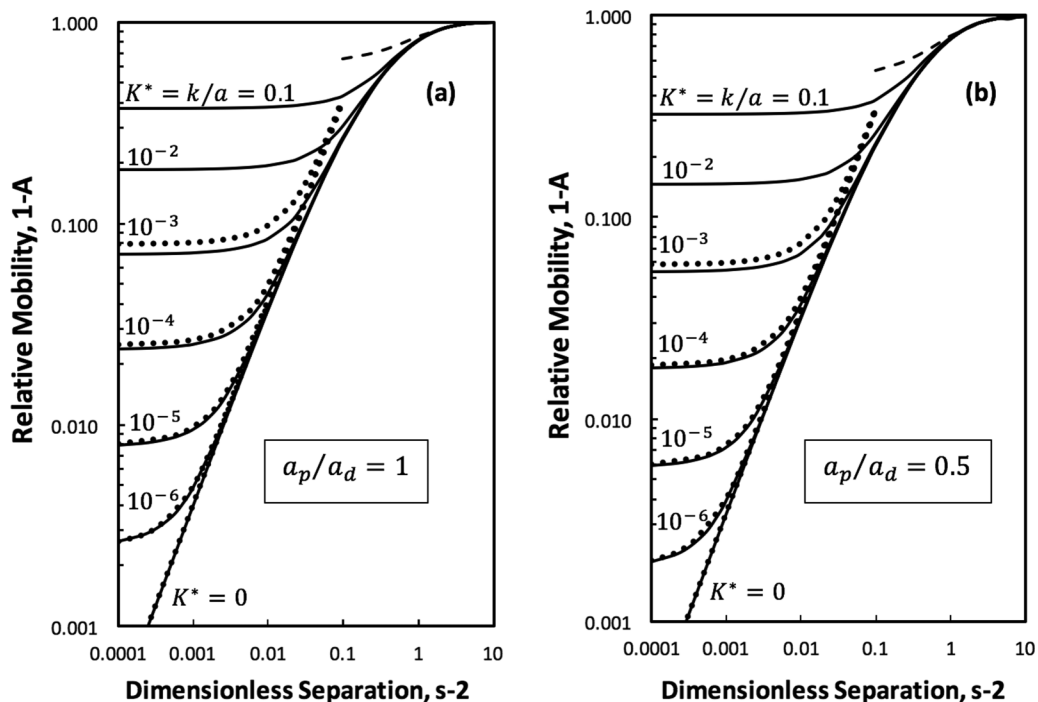


FIG. 4. Mobility function along the line-of-centers for a spherical solid particle approaching a spherical permeable drop due to a linear flow field. The solid curves are numerical results using bispherical coordinates, the dashed curves are the far-field results for impermeable spheres using Eq. (45), and the dotted lines are the near-field results using Eq. (51) for  $K^* \ll 1$ .

$s - 2$  as the gap becomes small. The asymptotic prediction of Eq. (63) for touching is in excellent agreement with the numerical results for  $1 - A_0$  when  $K^* \lesssim 10^{-3}$  (as is typically expected in practice), but then begins to deviate for larger dimensionless permeabilities because there is no longer a significant lubrication resistance to close approach, as required by Eq. (51) and, hence, Eq. (63).

The quantity  $C_1$  introduced in Eq. (47) is the ratio of the relative mobility due to an external flow pushing two nearly touching spheres together to that when the spheres are pulled together by an equal and opposite force. Table II shows  $C_1$  to be a strong function of the size ratio but only a weak function of the permeability. The latter is because permeation has the same effect on the near-contact lubrication force in the two cases, but a slightly different effect on the hydrodynamic forces on the sphere surfaces away from the lubrication region. In contrast, the numerical values of  $1 - A_0$  in Table II show a strong dependence on the permeability, as expected from Eq. (63). Note that the mobility functions for the impermeable case are unchanged when  $\lambda$  is replaced by  $1/\lambda$  (due to a simple relabeling of the two spheres), but not when permeation is present for only one sphere. The difference is small, however, for  $K^* \ll 1$ . The function  $f(\text{Pm})$ , also required for the near-field Eqs. (51) and (63), is the ratio of the lubrication force with permeation to that without permeation. It is determined by numerical solution of the dimensionless form of Eq. (55), via superposition of two initial-value problems, with the results shown in Fig. 5 and also as the inset to Fig. 3 of Ramon *et al.* [14]. Remarkably, the asymptotic expansions of Ramon *et al.* [14] for  $\text{Pm} \ll 1$  and  $\text{Pm} \gg 1$  nearly overlap, thus almost covering the full range of modified permeabilities,  $\text{Pm} = ak/h_0^2$ . In particular, (59) is accurate within 2% for  $\text{Pm} < 0.2$  and Eq. (61) is accurate within 2% for  $\text{Pm} > 0.6$ .

Figure 6 shows the relative mobility function normal to the line-of-centers, plotted as  $1 - B(s)$  versus  $s - 2$  for different radius ratios and permeabilities. The far-fields expansions are again

TABLE II. Numerical values of the constants use in near-field expressions for the two-sphere relative mobility functions in linear flows.

$\lambda$	$K^*$	$C_1$	$1 - A_0$	$C_1(3K^*/2)^{1/2}$	$B_0$	$B_1$
0.25	0	0.7125	0	0	0.809	-1.60
0.25	$10^{-6}$	0.7126	0.00087	0.00087	0.705	-0.73
0.25	$10^{-5}$	0.7128	0.00273	0.00276	0.685	-0.675
0.25	$10^{-4}$	0.7136	0.00852	0.00874	0.6622	-0.624
0.25	$10^{-3}$	0.7162	0.02596	0.02774	0.6345	-0.585
0.25	0.01	0.7260	0.07522	0.08892	0.6055	-0.560
0.25	0.10	0.7697	0.1941	0.29810	0.5769	-0.525
0.5	0	1.518	0	0	0.549	-1.16
0.5	$10^{-6}$	1.518	0.00185	0.00186	0.5033	-0.789
0.5	$10^{-5}$	1.517	0.00580	0.00588	0.4938	-0.755
0.5	$10^{-4}$	1.517	0.01793	0.01858	0.4832	-0.726
0.5	$10^{-3}$	1.515	0.05341	0.05868	0.4707	-0.695
0.5	0.01	1.511	0.1459	0.1851	0.4576	-0.671
0.5	0.10	1.506	0.3252	0.5833	0.4481	-0.657
0.75	0	1.933	0	0	0.4197	-0.772
0.75	$10^{-6}$	1.933	0.00236	0.00237	0.4145	-0.735
0.75	$10^{-5}$	1.933	0.00738	0.00749	0.4116	-0.718
0.75	$10^{-4}$	1.931	0.02271	0.02365	0.4089	-0.707
0.75	$10^{-3}$	1.927	0.06700	0.07463	0.4067	-0.703
0.75	0.01	1.914	0.1784	0.2344	0.4046	-0.698
0.75	0.10	1.876	0.3743	0.7266	0.4053	-0.698
1.0	0	2.039	0	0	0.3921	-0.702
1.0	$10^{-6}$	2.039	0.00248	0.00250	0.3921	-0.702
1.0	$10^{-5}$	2.038	0.00777	0.00789	0.3921	-0.702
1.0	$10^{-4}$	2.036	0.02389	0.02494	0.3921	-0.703
1.0	$10^{-3}$	2.031	0.07022	0.07866	0.3921	-0.703
1.0	0.01	2.014	0.1850	0.2467	0.3927	-0.705
1.0	0.10	1.960	0.3774	0.7591	0.3966	-0.714
2.0	0	1.518	0	0	0.549	-1.16
2.0	$10^{-6}$	1.517	0.00185	0.00186	0.5033	-0.789
2.0	$10^{-5}$	1.517	0.00579	0.00588	0.4938	-0.756
2.0	$10^{-4}$	1.516	0.01782	0.01857	0.4830	-0.726
2.0	$10^{-3}$	1.512	0.05248	0.05856	0.4705	-0.699
2.0	0.01	1.496	0.1384	0.1832	0.4578	-0.687
2.0	0.10	1.443	0.2766	0.5589	0.4515	-0.696

accurate for  $s - 2 \gtrsim 1$ , and there is very little change with permeability. The effect of permeation on  $B(s)$  is very small for  $\lambda = 1$ , even at small separations. However, the effect is pronounced for disparate sizes at small separations. In particular, the relative mobility  $1 - B(s)$  increases with increasing  $K^*$ , as was also seen with  $1 - A(s)$ , indicating that permeation reduces the resistance to relative motion. The constants  $B_0$  and  $B_1$  used in Eq. (61) for the near-field expression are included in Table II.

### B. Collision efficiency

Finally, the  $A(s)$  and  $B(s)$  mobility functions were used to determine the collision efficiency for uniaxial extensional flow (the same results apply for uniaxial compression). In addition to

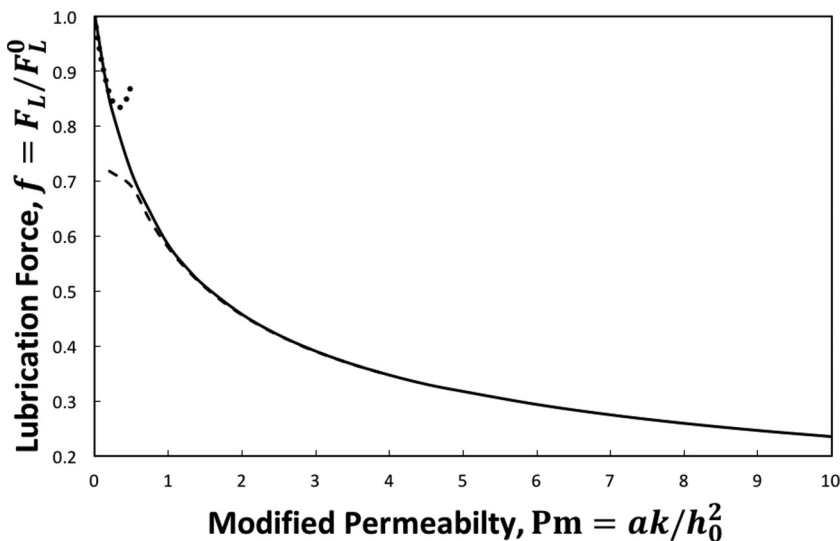


FIG. 5. Lubrication force for a solid particle interacting with a permeable drop, normalized by that for two solid particles. The solid curve is the numerical solution, the dotted curve is from Eq. (59), and the dashed curve is from Eq. (61).

employing Eqs. (8) and (9) directly, we used the trajectory approach of starting at the grazing point ( $s = 2$ ,  $\theta = \arctan(\sqrt{2})$ ) and integrated Eq. (6) backwards (decreasing  $\theta$ ) until the separation became large enough ( $s \approx 5 - 10$ ) that hydrodynamic interactions were negligible, allowing for the

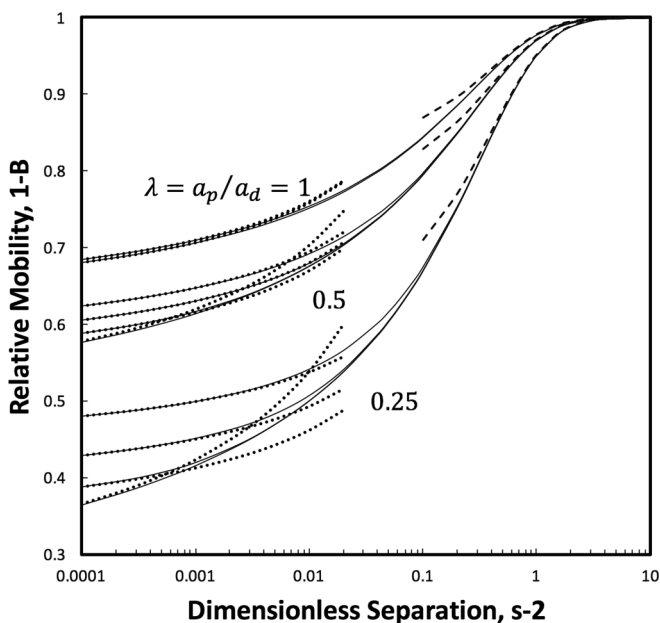


FIG. 6. Relative mobility function normal to the line-of-centers for a spherical particle approaching a permeable drop in a linear flow field. The solid curves are numerical results using bispherical coordinates, and the dashed curve is the far-field result for impermeable spheres using Eq. (47). For each size ratio, results are shown for  $K^* = 0$  (bottom curve) and  $0.1$  (top curve), with  $K^* = 10^{-3}$  and  $10^{-5}$  also included for  $\lambda = 0.5$  and  $0.25$ .

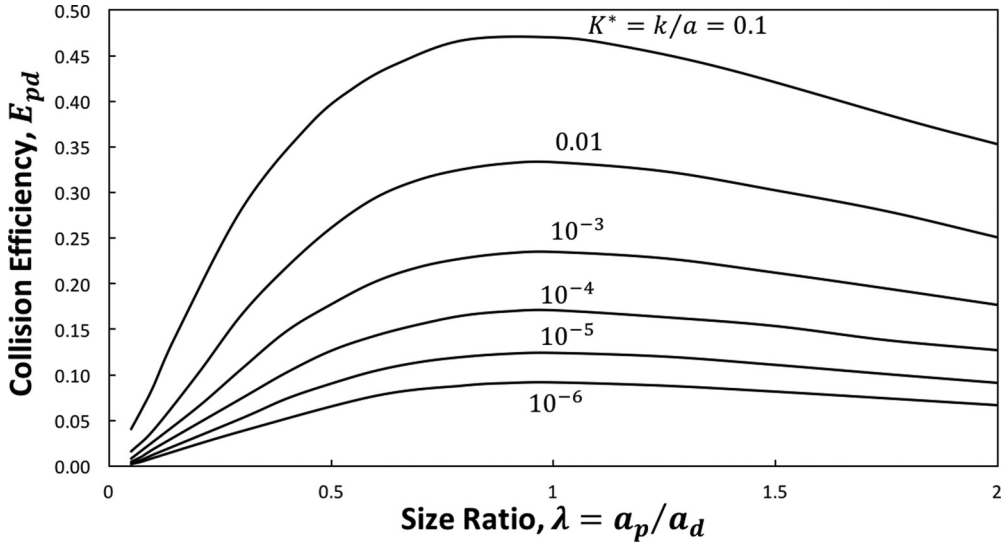


FIG. 7. Collision efficiency of a solid, spherical particle and a permeable, spherical drop in uniaxial extensional flow versus size ratio for different dimensionless permeabilities.

interception area to be determined along with the flux of particles through the interception area from Eq. (3). The two methods gave the same results. Figure 7 shows the resulting collision efficiency as a function of the size ratio and dimensionless permeability. As noted previously, the collision efficiency is identically zero in the absence of permeation, due to the resistance to close approach from the singular lubrication force Eq. (55). Even a small amount of permeation, however, allows

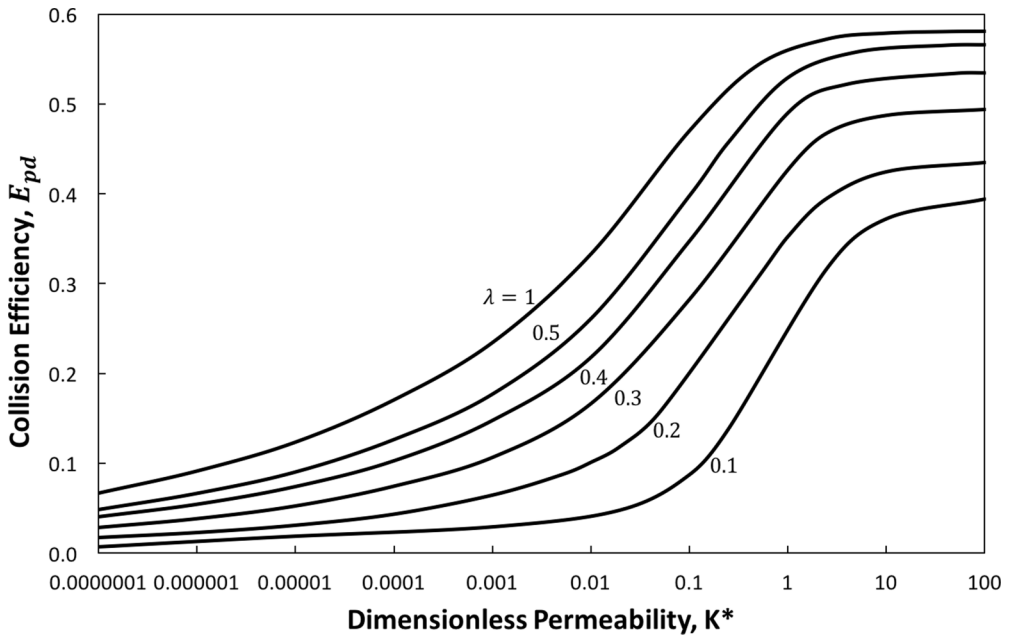


FIG. 8. Collision efficiency of a solid, spherical particle and a permeable, spherical drop in uniaxial extensional flow versus dimensionless permeability for different size ratios.

the spheres to make contact, resulting in surprisingly large collision efficiencies (e.g.,  $E_{pd} = 0.09$  for  $K^* = 10^{-6}$ , 0.17 for  $K^* = 10^{-4}$  and 0.23 for  $K^* = 0.001$ , when  $\lambda = 1$ ). The results for  $1/\lambda$  are nearly (but not identically) the same as for  $\lambda$ . When  $\lambda \ll 1$ , the small particle nearly follows the fluids streamlines around the larger drop, and so the collision efficiency is small due to the low fraction of streamlines that pass within one particle radius of the drop surface. Similarly, the collision efficiency is small for  $\lambda \gg 1$ , as the small droplet is swept by the fluid streamlines around the larger drop. Thus, there is a shallow maximum in the collision efficiency at a size ratio near  $\lambda = 1$ .

Figure 8 recasts the collision efficiency for uniaxial extension or compression as a function of the dimensionless permeability for different size ratios. The results are sigmoidal shape on this semilog plot. The collision efficiencies slowly increase with  $1/\log(1/K^*)$  for  $K^* \lesssim 10^{-3}$ , then rapidly increase for  $10^{-3} \lesssim K^* \lesssim 1$ , and level out or saturate for  $K^* \gtrsim 10$ .

## V. CONCLUDING REMARKS

This work has considered the collisions of small solid particles with membrane-covered droplets when immersed in a linear flow field under conditions of negligible inertia and Brownian motion. The two-sphere relative mobility functions for the hydrodynamic interactions for motion along and normal to the line-of-centers were calculated using bispherical coordinates for arbitrary separation distance, size ratios, and membrane permeabilities. The latter is described by the dimensionless parameter  $K^* = k/a$ , where  $k$  is the membrane permeance (or permeability per unit thickness), and  $a$  is the reduced radius of the two spheres. Under typical conditions, it is anticipated that  $K^* \ll 1$ . The numerical solution is supplemented by analytical expressions for large and small separations. The mobility functions were then used in a trajectory analysis to calculate the collision efficiency in uniaxial extension or compression, defined as the collision rate in a dilute suspension with hydrodynamic interactions to that in their absence.

As shown previously for a sphere approaching a flat membrane [12–14], a key result is that a nonzero relative velocity along the line-of-centers continues all the way to contact due to permeation. This result is in contrast to rigid, impermeable spheres, for which the relative velocity goes to zero as contact is approached due to a finite flow or force. The value of the relative mobility function along the line-of-centers is  $1 - A = (3K^*/2)^{1/2}$  at touching for  $K^* \ll 1$ , in agreement with lubrication theory [14]. As a consequence, the collision efficiency with permeation is nonzero, while that without permeation is zero (unless other effects, such as surface roughness or van der Waals attractions are included in the analysis). The collision efficiencies are surprisingly large, in the range of 0.1–0.5 for  $K^* = 10^{-6}$ –0.1 for particles and drops of equal size, even though permeation is only important at small separations (where lubrication pressure in the narrow gap pushes fluid across the membrane).

For future work, we are interested in the case where the membrane is expandable (such as for a water drop covered with a thin hydrocarbon layer) and there is an osmotic force that drives permeation into the drop. In this case, the drop will expand and may engulf nearby particles, further contributing to the collision rate. Also of interest is predicting the collision efficiency of two drops with permeable films, as coalescence would then affect the drop-size distribution.

## ACKNOWLEDGMENTS

The authors thank Professor Kevin Galvin of the University of Newcastle for introducing them to the application of particle agglomeration by permeable, oil-covered drops. We also thank Sydney Baysinger and Noemi Collado for assisting with the calculations and preparation of figures. This work was supported, in part, by a seed grant from the University of Colorado and a grant from the Australian Research Council (Grant No. DP180101617).

**APPENDIX: DETAIL OF THE BISPHERICAL-COORDINATE  
SOLUTION OF PROBLEM 2**

For the drop and particle in shear flow  $\mathbf{v}_\infty(\mathbf{x}) = (Gz, 0, 0)$ , the functions  $f_n(\eta)$ ,  $\varphi_n(\eta)$  and  $\psi_n(\eta)$  between the spheres and inside the drop still have Eqs. (16) and (18), but the ambient flow representation is now different:

$$\varphi_n^\infty(\eta) = 0, \quad \psi_n^\infty(\eta) = \pm Gc\sqrt{2}(2n+1)\exp[-(n+1/2)|\eta|], \quad (\text{A1})$$

where, again, the upper sign is taken for  $\eta > 0$ , and the lower sign for  $\eta < 0$ . Additionally,

$$\begin{aligned} \chi_n^e(\eta) &= G_n^e \exp[(n+1/2)(\eta - \eta_p)] + H_n^e \exp[(n+1/2)(\eta_d - \eta)], \\ \chi_n^i(\eta) &= G_n^i \exp[(n+1/2)(\eta - \eta_p)]. \end{aligned} \quad (\text{A2})$$

With so-defined coefficients, the flow incompressibility between the spheres and inside the drop requires [21]:

$$\begin{aligned} 5C_n^e - (n-1)e^{\eta_p}C_{n-1}^e + (n+2)e^{-\eta_p}C_{n+1}^e - 2(n-1)e^{\eta_p}A_{n-1}^e - 2(n+2)e^{-\eta_p}A_{n+1}^e + 2(2n+1)A_n^e \\ + 2E_n^e - e^{\eta_p}E_{n-1}^e - e^{-\eta_p}E_{n+1}^e - 2(n-1)(n+2)G_n^e + (n-2)(n-1)e^{\eta_p}G_{n-1}^e \\ + (n+2)(n+3)e^{-\eta_p}G_{n+1}^e = 0, \end{aligned} \quad (\text{A3})$$

$$\begin{aligned} 5D_n^e - (n-1)e^{-\eta_d}D_{n-1}^e + (n+2)e^{\eta_d}D_{n+1}^e + 2(n-1)e^{-\eta_d}B_{n-1}^e + 2(n+2)e^{\eta_d}B_{n+1}^e - 2(2n+1)B_n^e \\ + 2F_n^e - e^{-\eta_d}F_{n-1}^e - e^{\eta_d}F_{n+1}^e - 2(n-1)(n+2)H_n^e + (n-2)(n-1)e^{-\eta_d}H_{n-1}^e \\ + (n+2)(n+3)e^{\eta_d}H_{n+1}^e = 0, \end{aligned} \quad (\text{A4})$$

$$\begin{aligned} 5C_n^i - (n-1)e^{\eta_p}C_{n-1}^i + (n+2)e^{-\eta_p}C_{n+1}^i - 2(n-1)e^{\eta_p}A_{n-1}^i - 2(n+2)e^{-\eta_p}A_{n+1}^i + 2(2n+1)A_n^i \\ + 2E_n^i - e^{\eta_p}E_{n-1}^i - e^{-\eta_p}E_{n+1}^i - 2(n-1)(n+2)G_n^i + (n-2)(n-1)e^{\eta_p}G_{n-1}^i \\ + (n+2)(n+3)e^{-\eta_p}G_{n+1}^i = 0, \end{aligned} \quad (\text{A5})$$

for all  $n \geq 1$ .

The velocity continuity on the drop surface yields:

$$\Delta f_n = \frac{2}{\sinh \eta_d} \left[ \frac{(n-1)Z_{n-1}}{2n-1} + \frac{(n+2)Z_{n+1}}{2n+3} - Z_n \cosh \eta_d \right], \quad n \geq 1, \quad (\text{A6})$$

$$\psi_n^i(\eta_d) - \psi_n^e(\eta_d) = \frac{1}{\sinh \eta_d} \left[ \frac{(n+1)(n+2)Z_{n+1}}{2n+3} - \frac{n(n-1)Z_{n-1}}{2n-1} \right], \quad n \geq 0, \quad (\text{A7})$$

$$\chi_n^i(\eta_d) - \chi_n^e(\eta_d) = \frac{1}{\sinh \eta_d} \left( \frac{Z_{n-1}}{2n-1} - \frac{Z_{n+1}}{2n+3} \right), \quad n \geq 2, \quad (\text{A8})$$

where

$$Z_n = \varphi_n^i(\eta_d) - \varphi_n^e(\eta_d), \quad \Delta f_n = f_n^i(\eta_d) - f_n^e(\eta_d). \quad (\text{A9})$$

Using Eqs. (A6)–(A8) and the definitions Eqs. (16), (18) (A2), and (A9), the internal coefficients  $A_n^i$ ,  $C_n^i$ ,  $E_n^i$ , and  $G_n^i$  can be expressed via the external  $A_n^e \dots H_n^e$  coefficients and  $Z_m$  (with  $n-1 \leq m \leq n+1$ ). Substituting such expressions into Eq. (A5) and combining it with Eq. (A3) replace the

continuity equation for the internal flow by

$$\begin{aligned}
 & 5D_n^e - (n-1)e^{\eta_d} D_{n-1}^e + (n+2)e^{-\eta_d} D_{n+1}^e - 2(n-1)e^{\eta_d} B_{n-1}^e - 2(n+2)e^{-\eta_d} B_{n+1}^e \\
 & + 2(2n+1)B_n^e + 2F_n^e - e^{\eta_d} F_{n-1}^e - e^{-\eta_d} F_{n+1}^e - 2(n-1)(n+2)H_n^e \\
 & + (n-2)(n-1)e^{\eta_d} H_{n-1}^e + (n+2)(n+3)e^{-\eta_d} H_{n+1}^e \\
 & + \frac{4}{\sinh \eta_d} \left[ \frac{(n-1)Z_{n-1}}{2n-1} + \frac{(n+2)Z_{n+1}}{2n+3} - \left( \cosh \eta_d + \frac{\sinh \eta_d}{2n+1} \right) Z_n \right] = 0, \quad n \geq 1, \quad (\text{A10})
 \end{aligned}$$

where the internal flow coefficients are present only through  $Z_m$ .

For convenient implementation of the remaining boundary conditions on the drop surface, consider the fluid velocity  $\tilde{\mathbf{v}}^d = \mathbf{v}^e - \mathbf{V}_d - \boldsymbol{\omega}_d \times (\mathbf{x} - \mathbf{x}_d)$  of the carrier fluid near the sphere  $\eta = \eta_d$  in the reference frame moving with the membrane;  $\mathbf{x}_d$  is the drop center. This velocity is still represented by Eqs. (35) and (36), with  $\psi_n^e(\eta)$  and  $\varphi_n^e(\eta)$  in Eq. (16) replaced, respectively, by

$$\tilde{\psi}_n^d(\eta) = \psi_n^e(\eta) - V_d \sqrt{2} \exp[(n+1/2)\eta] + \omega_d c \sqrt{2} (2n+1 + \coth \eta_d) \exp[(n+1/2)\eta] \quad (\text{A11})$$

and

$$\tilde{\varphi}_n^d(\eta) = \varphi_n^e(\eta) + \omega_d c \sqrt{2} \exp[(n+1/2)\eta]. \quad (\text{A12})$$

The boundary condition of zero tangential relative velocity  $\tilde{v}_\xi^d = \tilde{v}_\theta^d = 0$  yields two equations:

$$\begin{aligned}
 & \frac{n(n-1)}{2n-1} [f_{n-1}^e \cosh \eta + 2\tilde{\varphi}_{n-1}^d \sinh \eta] - \frac{(n+1)(n+2)}{2n+3} [f_{n+1}^e \cosh \eta + 2\tilde{\varphi}_{n+1}^d \sinh \eta] \\
 & + 2 \cosh \eta \left[ \frac{(n+1)\tilde{\psi}_{n+1}^d}{2n+3} + \frac{n\tilde{\psi}_{n-1}^d}{2n-1} \right] - 2\tilde{\psi}_n^d = 0 \quad \text{at} \quad \eta = \eta_d, \quad n \geq 0, \quad (\text{A13})
 \end{aligned}$$

and

$$\begin{aligned}
 & \frac{f_{n+1}^e \cosh \eta + 2\tilde{\varphi}_{n+1}^d \sinh \eta}{2n+3} - \frac{f_{n-1}^e \cosh \eta + 2\tilde{\varphi}_{n-1}^d \sinh \eta}{2n-1} \\
 & + 2 \left[ \frac{(n-2)\chi_{n-1}^e}{2n-1} + \frac{(n+3)\chi_{n+1}^e}{2n+3} \right] \cosh \eta - 2\chi_n^e = 0 \quad \text{at} \quad \eta = \eta_d, \quad n \geq 2. \quad (\text{A14})
 \end{aligned}$$

The permeability boundary condition on the drop surface,  $\tilde{v}_\eta^e = 2\gamma[F^i - F^e] \cos \theta$ , used together with  $\tilde{v}_\theta = 0$ , results in

$$\begin{aligned}
 & 2\tilde{\varphi}_n^d - \frac{n-1}{2n-1} [f_{n-1}^e \sinh \eta + 2\tilde{\varphi}_{n-1}^d \cosh \eta] - \frac{n+2}{2n+3} [f_{n+1}^e \sinh \eta + 2\tilde{\varphi}_{n+1}^d \cosh \eta] \\
 & + 2 \left[ \frac{\tilde{\psi}_{n+1}^d}{2n+3} - \frac{\tilde{\psi}_{n-1}^d}{2n-1} \right] \sinh \eta \\
 & = 2\gamma \left[ \Delta f_n \cosh \eta - \frac{n-1}{2n-1} \Delta f_{n-1} - \frac{n+2}{2n+3} \Delta f_{n+1} \right] \quad \text{at} \quad \eta = \eta_d, \quad n \geq 1. \quad (\text{A15})
 \end{aligned}$$

Near the solid particle surface  $\eta = \eta_p$ , we work, again, with the relative fluid velocity  $\tilde{\mathbf{v}}^p = \mathbf{v}^e - \mathbf{V}_p - \boldsymbol{\omega}_p \times (\mathbf{x} - \mathbf{x}_p)$ , where  $\mathbf{x}_p$  is the particle center. This velocity is still represented by Eqs. (35) and (36), with  $\psi_n^e(\eta)$  and  $\varphi_n^e(\eta)$  in Eq. (16) replaced, respectively, by

$$\tilde{\psi}_n^p(\eta) = \psi_n^e(\eta) - V_p \sqrt{2} \exp[-(n+1/2)\eta] - \omega_p c \sqrt{2} (2n+1 - \coth \eta_p) \exp[-(n+1/2)\eta] \quad (\text{A16})$$

and

$$\tilde{\varphi}_n^p(\eta) = \varphi_n^e(\eta) + \omega_p c \sqrt{2} \exp[-(n + 1/2)\eta]. \quad (\text{A17})$$

The no-slip boundary condition  $\tilde{\mathbf{v}}^p = \mathbf{0}$  gives three final equations:

$$f_n^e + \frac{2}{\sinh \eta} \left[ \tilde{\varphi}_n^p \cosh \eta - \frac{(n-1)\tilde{\varphi}_{n-1}^p}{2n-1} - \frac{(n+2)\tilde{\varphi}_{n+1}^p}{2n+3} \right] = 0 \quad \text{at } \eta = \eta_p, \quad n \geq 1, \quad (\text{A18})$$

$$\tilde{\psi}_n^p + \frac{1}{\sinh \eta} \left[ \frac{n(n-1)\tilde{\varphi}_{n-1}^p}{2n-1} - \frac{(n+1)(n+2)\tilde{\varphi}_{n+1}^p}{2n+3} \right] = 0 \quad \text{at } \eta = \eta_p, \quad n \geq 0, \quad (\text{A19})$$

$$\chi_n^e + \frac{1}{\sinh \eta} \left( \frac{\tilde{\varphi}_{n+1}^p}{2n+3} - \frac{\tilde{\varphi}_{n-1}^p}{2n-1} \right) = 0 \quad \text{at } \eta = \eta_p, \quad n \geq 2. \quad (\text{A20})$$

Equations (A3), (A4), (A6), (A10), (A13), (A14), (A15), (A18), (A19), and (A20), complemented by the definitions Eqs. (16), (A1), (A11), (A12), (A16), and (A17), present a compact form of ten difference equations for the solution vector  $\mathbf{X}_n = (A_n^e, B_n^e, C_n^e, D_n^e, E_n^e, F_n^e, G_n^e, H_n^e, Z_n, \Delta f_n)$ . This system can be written in a general form akin to Eq. (32), with shear rate  $G$  instead of  $E_{33}$ , and additional contributions in the right-hand side due to particle/drop membrane rotations. The limitations  $A_0^e = B_0^e = C_0^e = D_0^e = Z_0 = \Delta f_0 = 0$  and  $G_n^e = H_n^e = 0$  (for  $n \leq 1$ ) are used to extend this tridiagonal system to all  $n \geq 1$  and start the forward sweep  $\mathbf{X}_n = \mathbf{L}_n \mathbf{X}_{n+1} + \mathbf{K}_n$  of the Thomas algorithm, with recurrent calculation of matrices  $\mathbf{L}_n$  and vectors  $\mathbf{K}_n$ .

The hydrodynamic forces  $F_p, F_d$  (acting in the  $x$ -direction) and torques  $T_p, T_d$  about the particle/drop centers (acting in the  $y$  direction) are

$$F_p = -8\pi\mu c \sqrt{2} \sum_{n=0}^{\infty} E_n^e \exp[-(n + 1/2)\eta_p], \quad F_d = -8\pi\mu c \sqrt{2} \sum_{n=0}^{\infty} F_n^e \exp[(n + 1/2)\eta_d] \quad (\text{A21})$$

and

$$T_p = -8\pi\mu c^2 \sqrt{2} \sum_{n=0}^{\infty} (2n + 1 - \coth \eta_p) E_n^e \exp[-(n + 1/2)\eta_p],$$

$$T_d = 8\pi\mu c^2 \sqrt{2} \sum_{n=0}^{\infty} (2n + 1 - \coth \eta_d) F_n^e \exp[(n + 1/2)\eta_d]. \quad (\text{A22})$$

Again, the infinite series Eqs. (A21) and (A22) can be computed on the forward sweep as the limits of recurrent sequences with automatic convergence control, thus not requiring the solution vector  $\mathbf{X}_n$ .

For an impermeable drop near a particle at arbitrary separations, our solution of Problem 2 was found to be in perfect agreement with known bispherical-coordinate solutions for two solid spheres translating/rotating with prescribed velocities normal to the centerline in quiescent liquid [21], and with related solutions for two freely suspended solid spheres in a linear flow [5,18]. For finite drop permeabilities and very large surface separations, there was again perfect agreement with the analytical drag formula Eq. (34). The single drop test is still meaningful, because our algorithms for Problem 1 and Problem 2 are based on the vastly different flow representations Eqs. (14) and (35). Finally, our numerical values for the mobility function  $B$  are very accurately described by the far-field form Eq. (43), when the surface separation exceeds just a few particle/drop radii.

---

[1] A. Curtis and L. Hocking, Collision efficiency of equal spherical particles in a shear flow. The influence of London-van der Waals forces, *Trans. Faraday Soc.* **66**, 1381 (1970).

- [2] T. Van de Ven and S. Mason, The microrheology of colloidal dispersions, *Colloid Polym. Sci.* **255**, 794 (1977).
- [3] G. Zeichner and W. Schowalter, Use of trajectory analysis to study stability of colloidal dispersion in flow fields, *Amer. Inst. Chem. Eng. J.* **23**, 243 (1977).
- [4] P. Adler, Heterocoagulation in shear flow, *J. Colloid Interface Sci.* **83**, 106 (1981).
- [5] G. Batchelor and J. Green, The hydrodynamic interaction of two small freely-moving spheres in a linear flow field, *J. Fluid Mech.* **56**, 375 (1972).
- [6] A. Zinchenko, Hydrodynamic interaction of two identical liquid spheres in linear flow field, *J. Appl. Math. Mech.* **47**, 37 (1983).
- [7] H. Wang, A. Zinchenko, and R. Davis, The collision rate of small drops in linear flow fields, *J. Fluid Mech.* **265**, 161 (1994).
- [8] R. Davis, J. Schonberg, and J. Rallison, The lubrication force between two viscous drops, *Phys. Fluids* **1**, 77 (1989).
- [9] M. Rother and R. Davis, The effect of slight deformation on droplet coalescence in linear flows, *Phys. Fluids* **13**, 1178 (2001).
- [10] K. Van Netten, D. Borrow, and K. Galvin, Fast agglomeration of ultrafine hydrophobic particle using a high-internal-phase emulsion binder comprising permeable hydrophobic films, *Ind. Eng. Chem. Res.* **56**, 10658 (2017).
- [11] A. Davis, Axisymmetric flow due to a porous sphere sedimenting towards a solid sphere or a solid wall: Application to scavenging of small particles, *Phys. Fluids* **13**, 3126 (2001).
- [12] S. Goren, The hydrodynamic force resisting the approach of a sphere to a plane permeable wall, *J. Colloid Interface Sci.* **69**, 78 (1979).
- [13] A. Nir, On the departure of a sphere from contact with a permeable membrane, *J. Eng. Math.* **15**, 65 (1981).
- [14] G. Ramon, H. Huppert, J. Lister, and H. Stone, On the hydrodynamic interaction between a particle and a permeable surface, *Phys. Fluids* **25**, 73103 (2013).
- [15] L. Mir, S. Michaels, V. Goel, and R. Kaiser, *Membrane Handbook* (Springer, Boston, MA, 1992).
- [16] M. Smoluchowski, Experiments on a mathematical theory of kinetic coagulation of colloid solutions, *Z. Phys. Chem.* **92**, 129 (1917).
- [17] A. Zinchenko, Effect of hydrodynamic interactions between the particles on the rheological properties of dilute emulsions, *J. Appl. Math. Mech.* **48**, 198 (1984).
- [18] C. Lin, K. Lee, and N. Sather, Slow motion of two spheres in a shear field, *J. Fluid Mech.* **43**, 35 (1970).
- [19] A. Zinchenko, The slow asymmetric motion of two drops in a viscous medium, *J. Appl. Math. Mech.* **44**, 30 (1980).
- [20] M. Cooley and M. O'Neill, On the slow motion generated in a viscous fluid by the approach of a sphere to a plane wall or stationary sphere, *Mathematika* **16**, 37 (1969).
- [21] M. O'Neill and R. Majumdar, Asymmetrical slow viscous fluid motions caused by the translation or rotation of two spheres. Part I: The determination of exact solutions for any values of the ratio of radii and separation parameters, *Z. Angew. Math. Phys.* **21**, 164 (1970).